Korea-Australia Rheology Journal
Vol. 22, No. 3, September 2010 pp. 151-162

Modeling of flow-induced crystallization of colored polypropylene in injection molding

Rong Zheng[1,*], R. I. Tanner[1], D. Lee Wo[1], Xi-jun Fan[1], C. Hadinata[2], F.S. Costa[2],
P.K. Kennedy[3], P. Zhu[4] and G. Edward[4]
[1]*School of Aerospace, Mechanical and Mechatronic Engineering, The University of Sydney, NSW 2006, Australia*
[2]*Autodesk Pty Ltd., 259-261 Colchester Road, Kilsyth, Melbourne, VIC 3137,Australia*
[3]*95 Ormond Road, Elwood, VIC 3148, Australia*
[4]*Department of Materials Engineering, Monash University, Clayton, VIC 3800, Australia*
(Received November 19, 2009; final revision received February 8, 2010; accepted May 28, 2010)

Abstract

We present a study on flow-induced crystallization of an injection-molded isotactic polypropylene (iPP) mixed with colorant additives. Two types of blue colorants were used in the study: one is the ultramarine Blue composed of Sodium Alumino Sulpho Silicate (UB) and the other is the PV Fast Blue composed of Cu-Phthalocyanine (CuPc). The CuPc colorant exhibits increased nucleation of both quiescent and flow-induced crystallization, and results in more oriented microstructures, causing a high degree of anisotropy in material properties and shrinkage of the injection molded parts. In contrast, the nucleating effect of the UB colorant is negligible under the quiescent condition, but becomes notable in the case of short-term shear treatment at high shear rates. The UB colorant does not significantly increase the degree of anisotropy as compared with the virgin iPP. A flow-induced crystallization kinetic model is used in the numerical simulation for the injection molding process, and predicted the colorant effects as observed in experiments.

Keywords **:** crystallization, colorants, injection molding, shrinkage, morphology

1. Introduction

In the last two decades, significant progress has been made in the development of computer- aided engineering analysis for injection molding. Recent efforts have focused on linking the flow-induced crystallization (FIC) of semi-crystalline materials to the processing and the resulting material properties. In injection molding of semi-crystalline polymers, the molten polymer flow accelerates crystallization and may induce an oriented "shish-kebab" semicrystalline structure in the high shear rate regions (Eder and Janeschitz-Kriegl 1997; Zuidema, *et al*., 2001). Typically, the enhancement in polymer crystallization rate crucially changes the flow and solidification behavior, and the oriented microstructure leads to a local anisotropy in thermal and mechanical properties, which can further cause anisotropic shrinkage and hence enhanced warpage of the injection-molded parts.

Most injection molding simulations use data obtained for virgin materials, but to mould the parts, various colors are typically added and these are known to affect the rheological and crystallization behavior of the processed polymer, as reported by Silberman (1995), Hadinata *et al.* (2008), Zheng *et al.* (2008) and Zhu *et al.* (2009). There is still a lack of theory and methods for predicting these effects.

It is generally believed that the colorants, as foreign particles, promote the heterogeneous crystallization of polymers. Heterogeneous crystallization is activated on the surface of the foreign particles, while the effectiveness of the crystallization process depends on the surface patterns, pigment sizes and degree of aggregation and dispersion. Pigment particles come in a variety of forms, with primary particle sizes in the range 0.01mm to 1mm and with varying degrees of combination into aggregates or agglomerates, where the tightly packed aggregates reduce the pigment surface area for a given loading, whereas the loosely packed agglomerates do not affect the surface area exposed when compared to that of the primary particles.

Given the vast variety of colorants, both in chemical and physical properties, and in shape and geometrical arrangement, to include all the details in the numerical modeling is not straightforward, if not impossible. However, in a practical computation, the basic kinetic model for materials with and without colorants can remain the same, but the model parameters should be carefully determined for each colored polymer such that the nucleation and growth trends are correlated with the colorant effects. We will use this approach here.

---

*Corresponding author: rong.zheng@uni.sydney.edu.au

2. Theory

2.1. Flow-induced crystallization kinetics

Following the work of Kolmogoroff (1937) we first consider an unrestricted growth of crystals and calculate a fictive volume fraction. Let G denote the rate of growth of the spherulite radius as a function of time. The volume of a phantom spherulite, nucleated at the instant s and grown up to the instant t, is given by $\upsilon_1(s,t)=(4\pi/3)[\int_s^t G(u)du]^3$. The shish-kebab structure is represented by a cylindrical geometry. It is assumed by Eder and Janeschitz-Kriegl (1997) that the lateral growth rate is the same as the spherulite radial growth rate G, unaffected by flow. Its volume is $\upsilon_2(s,t)=\pi l_s[\int_s^t G(u)du]^2$, where l_s is the length of the shish at time t. Denoting the number density of the quiescent nuclei by N_q and the flow-induced nuclei number density by N_f, the unrestricted total volume fraction of phantom crystals at time t is then given by

$$\varphi(t)=\int_0^t \dot{N}_q(s)\upsilon_1(s,t)ds+\int_0^t \dot{N}_f(s)[\omega\upsilon_1(s,t)+(1-\omega)\upsilon_2(s,t)]ds \quad (1)$$

Here the first integral term on the right-hand side of the equation is the quiescent contribution. The second integral term is the contribution of the flow-induced crystallization, where we introduce a two-value weight function ω:

$$\omega=0 \quad \text{if} \quad \dot{\gamma}>1/\lambda_R \text{ and } \int_0^{t_s}\eta\dot{\gamma}^2 dt>w_c \quad (2)$$

otherwise $\omega=1$.

In Eq. (2), η is the shear viscosity, $\dot{\gamma}$ is the generalized shear rate defined as $\dot{\gamma}=\sqrt{2D_{ij}D_{ij}}$, with $D_{ij}=(1/2)(\partial u_i/\partial x_j+\partial u_j/\partial x_i)$ being the rate-of-deformation tensor, λ_R is the longest Rouse time in the melt, t_s is the shearing time, the integration gives the specific work done on the sheared polymer, and w_c is the critical specific work. Related to this is the observation of Mykhaylyk *et al.* (2008) that the transition from isotropic spherulites to oriented shish-kebabs takes place at a critical amount of work. The magnitude of λ_R can be estimated by (Doi and Edwards 1986) $\lambda_R=\lambda_e(M/M_e)^2$, where M is the molecular weight of the high molecular weight chains, M_e is the entanglement molecular weight, and λ_e is the equilibration time. Literature data for M_e and λ_e are available for iPP (van Meerveld 2004): $M_e=4.4\text{kg/mol}$ and $\lambda_e=3.54\times10^{-8}$ s at $T=463$ K, and time-temperature superposition is applied to shift λ_e to other temperatures. Literature data for M/M_e are also summarized by van Meerveld *et al.* (2004)

In order to account for impingement, the fictive volume fraction should be converted to the actual relative crystallinity, α, which is also called the degree of space filling, defined as the ratio of crystallized volume at a given time to the total crystallizable volume. According to Kolmogoroff (1937) and Avrami (1939),

$$\alpha=1-\exp(-\varphi) \quad (3)$$

The growth rate of the spherulite radius G is calculated by applying Hoffman-Lauritzen theory (Lauritzen and Hoffman 1960)

$$G(T)=G_0\exp\left[-\frac{U^*}{R_g(T-T_\infty)}\right]\exp\left[-\frac{K_g(T+T_m^0)}{2T^2\Delta T}\right] \quad (4)$$

where G_0 and K_g are constants that can be determined by experiments under quiescent conditions, U^* is the activation energy of motion, often taken as a generic value of 6270 J/mol for iPP (*e.g*., Koscher and Fulchiron 2002), R_g is the gas constant, $T_\infty=T_g-30$ where T_g is the glass transition temperature and $\Delta T=T_m^0-T$ is the degree of supercooling with T_m^0 being the equilibrium melting temperature which is assumed to depend on pressure. The pressure dependence is represented by a polynomial function as

$$T_m^0(P)=a_0+a_1P+a_2P^2 \quad (5)$$

where a_i, $i\in\{0,1,2\}$ are constants and can be determined from the Pressure-Volume-Temperature diagram (Fulchiron *et al*., 2001), and P is the pressure.

The quiescent nuclei number is assumed to take the form $N_q=N_0H(t)$, with $H(t)$ being the Heaviside unit step function, zero for $t<0$ and unity for $t\geq0$. In the isothermal case, one has $\dot{N}_q=N_0\delta(t)$, with $\delta(t)$ being the Dirac delta function concentrated at $t=0$. Under quiescent and isothermal conditions, Eqs. (1) and (3) lead to the familiar Avrami equation:

$$\alpha(t)=1-\exp\left(-\frac{4\pi}{3}N_0G^3t^3\right) \quad (6)$$

According to Koscher and Fulchiron (2002), the value of N_0 has an exponential dependence on the degree of supercooling ΔT:

$$\ln N_0=a_N\Delta T+b_N \quad (7)$$

where a_N and b_N are constants to be determined experimentally.

The flow-induced nuclei number takes the form:

$$\dot{N}_f+\frac{1}{\lambda_N}N_f=f \quad (8)$$

where λ_N is a nucleation relaxation time which, according to Eder and Janeschitz-Kriegl (1997), has a large value and may vary with temperature, and f is a function of flow variables. Several expressions for the function f have been proposed by different authors based on different assumptions about the driving force for the enhancement of nucleation (see, for example, Eder and Janeschitz-Kriegl, 1997; Zuidema, 2001; Coppola et al., 2001; Koscher and Fulchiron, 2002; Zheng and Kennedy, 2004; Dai *et al*., 2006). Tanner and Qi (2005) and Pantani *et al.* (2005) have reviewed various theories. This study follows the previous work of Zheng and Kennedy, taking f as a function of the flow-induced change in the dumbbell free energy, ΔF_f, via the conformation tensor $\boldsymbol{c} = H<\boldsymbol{QQ}>k_B T$, where H is the spring elastic constant and $\boldsymbol{Q}$ is the end-to-end vector of a FENE-P dumbbell, and k_B is Boltzmann's constant. The reader is referred to the original paper for the model formulations. It is instructive to recall the asymptotic behavior of the driving force at the shearing flow. For low shear rates, the change in free energy due to flow is

$$\Delta F_f \approx \frac{1}{2} n_0 k_B T \left(\frac{b}{b+3}\right)^2 (Wi)^2 \tag{9}$$

and for high shear rate, one has

$$\Delta F_f \approx \frac{1}{3} n_0 k_B T (b-2) \ln(Wi) \tag{10}$$

where n_0 is the number density of the molecules (a quantity normally thought as being folded into a shear modulus that can be estimated or measured), b is the FENE-P model parameter (Detailed discussions on the parameter can be found in Fan (1985). In this work we use $b=5$ for all cases), and Wi is the Weissenberg number, *i.e.*, the generalized shear rate multiplied by the polymer relaxation time.

The number density of active nuclei (N_a) at the end of the crystallization process can be estimated by

$$N_a = \int_0^{t_{end}} \dot{N}(t)[1-\alpha(t)]dt \tag{11}$$

where N is the sum of the quiescent nuclei number density and the flow-induced nuclei number density, *i.e.*,

$$N = N_q + N_f \tag{12}$$

and the final average volume of the spherulites and shish-kebabs is

$$\bar{V} = \frac{\alpha}{N_a} \tag{13}$$

2.2. Effect of crystallinity on rheology

Injection molding flows are dominated by viscometric flow. The choice of different types of constitutive equations has only a minor influence on the flow kinematics (with exceptions near corners, at the flow front, and in regions of the mold with abrupt thickness variation), provided the shear viscosity is accurately described. In this study we choose to use the generalized Newtonian fluid constitutive model with a crystallinity-dependent viscosity, η. The extra stress tensor is given by

$$\tau_{ij} = 2\eta(\dot{\gamma}, T, P, \alpha) D_{ij} \tag{14}$$

Here we assume that the way crystallization affects rheology can be described by the suspension theory, following the idea of Tanner (2003). We express the viscosity ratio η/η_a by

$$\frac{\eta(\dot{\gamma}, T, P, \alpha)}{\eta_a(\dot{\gamma}, T, P)} = 1 + \frac{(\alpha/A)^{\beta_1}}{(1-\alpha/A)^{\beta}}, \quad a<A \tag{15}$$

where η_a is the viscosity of the amorphous phase, β and β_1 are the fitting parameters, A is set to 0.44, corresponding to rough and compact inclusions.

The resulting kinematics from the generalized Newtonian fluid will be used subsequently in a combination of a FENE-P fluid model and a rigid dumbbell model to calculate flow-induced free energy change, residual stresses and orientation.

2.3. Effect of crystallinity on pressure- volume-temperature behavior

In the simulation of injection molding, understanding and modeling of the pressure-volume-temperature (PVT) behavior of the material is essential. The PVT behavior is usually expressed in terms of the specific volume v as a function of temperature T and pressure P. The particularity of PVT behavior for semi-crystalline polymer is that the transition region between the liquid and the solid states is strongly influenced by the crystallization, thus the specific volume should also be a function of the relative crystallinity. The specific volume $v(T, P, \alpha)$ can be written as

$$v = [(1-\alpha)v_a^{-1} + \alpha v_s^{-1}]^{-1} \tag{16}$$

where $v_a = v_a(T, P)$ is the specific volume of the amorphous phase, $v_s = v_s(T, P, \chi_\infty)$ is the specific volume of the solid semi-crystalline polymer, and χ_∞ is the ultimate absolute crystallinity at the end of the solidification. Let v_c denote the specific volume of the pure crystalline phase, the specific volume of the solid polymer can be expressed by

$$v_s = [(1-\chi_\infty)v_a^{-1} + \chi_\infty v_c^{-1}]^{-1} \tag{17}$$

As v_s can be determined from the available PVT data, the value of χ_∞ does not need to be used in this calculation. The specific volumes v_a and v_s can be described by the Tait equation,

$$v_x = v_0(T)\left[1 - C\ln\left(1 + \frac{P}{B(T)}\right)\right] \tag{18}$$

where v_x represents either v_a or v_s, $C = 0.0894$ is a universal constant, and $v_0(T)$ is given by

$$v_0(T) = \begin{cases} b_1^{(a)} + b_2^{(a)}(T-b_5), & \text{for } v_x = v_a \\ b_1^{(s)} + b_2^{(s)}(T-b_5), & \text{for } v_x = v_s \end{cases} \tag{19}$$

and $B(T)$ is given by

$$B(T) = \begin{cases} b_3^{(a)} \exp[-b_4^{(a)}(T-b_5)], & \text{for } v_x = v_a \\ b_3^{(s)} \exp[-b_4^{(s)}(T-b_5)], & \text{for } v_x = v_s \end{cases} \tag{20}$$

2.4. Effect of crystallinity on thermal conductivity

In classical Fourier theory, thermal conductivity is assumed to be constant or dependant on the temperature alone. However, the theory is inadequate to describe the heat conduction in deformed molten polymer, where the thermal conductivity may depend on cooling rate and can also become anisotropic since the heat transport along the polymer back chain is considered to be more efficient than between neighboring chains. Moreover, the final conductivity may depend on the morphology after processing. Thus one has to consider the non-Fourier law (Huilgol *et al.*, 1992). To account for anisotropy, the thermal conductivity must be in tensor form as

$$q_i = k_{ij}\frac{\partial T}{\partial x_j} \tag{21}$$

where $\boldsymbol{q}$ (q_i) is the heat flux and $\boldsymbol{k}$ (k_{ij}) is the thermal conductivity tensor. Van den Brule (1989) suggested that, for amorphous polymers, there might be the following connection between the thermal conductivity tensor $\boldsymbol{k}$ and the total stress tensor $\boldsymbol{\sigma}$ (σ_{ij}):

$$k_{ij} - \frac{1}{3}k_{kk}\delta_{ij} = C_t k_0\left(\sigma_{ij} - \frac{1}{3}\sigma_{kk}\delta_{ij}\right) \tag{22}$$

where k_0 is the equilibrium scalar thermal conductivity, δ_{ij} is the unit tensor, and C_t is the stress-thermal coefficient. Dai and Tanner (2006) suggested that the same theory may be used for sheared semi-crystalline materials, with an enhanced value of C_t depending on the increased crystallinity. The idea of Dai and Tanner was implemented by Zheng and Kennedy (2006) in an injection molding simulation, but they also consider the dependence of k_0 on crystallinity. The following simple expression is assumed:

$$\frac{1}{k_0(\alpha, T)} = \frac{\alpha}{k_0^{(s)}(T)} + \frac{1-\alpha}{k_0^{(a)}(T)} \tag{23}$$

where α is the relative crystallinity, the superscripts (s) and (a) denote the solid state and the liquid amorphous state, respectively. The equilibrium scalar thermal conductivity at the solid state and the liquid amorphous state, both as a function of temperature can be measured experimentally.

The component of the thermal conductivity tensor in the gap-wise direction, k_{33}, decreases with increasing shear stresses according to the original van den Brule theory. However, the experiments for the iPP in this study showed an increase of k_{33} with increasing shear stresses. The latter effect could be due to the changed microstructure. The modified van den Brule formulation, with the crystallinity-dependent C_t and k_0, is able to describe the experimentally observed phenomenon mentioned above.

2.5. Governing equations for injection molding modelling

For injection molding modeling, we use the two-dimensional Hele-Shaw equation and the three-dimensional energy equation as described by Kennedy (1995), but with crystallinity-dependent viscosity, density and thermal properties. The effect of latent heat of fusion on temperature due to crystallization is also considered.

In order to predict dimension and shape of the final products, one also needs to calculate residual stresses. There are two sources of residual stresses. One is the flow-induced stresses, which are built up during the filling stage and later locked into the frozen layer due to the rapid increased relaxation time during crystallization. The frozen-in stresses can be calculated by subsequently solving a combined equation of a viscoelastic model and a rigid dumbbell model as mentioned above (such a “two-phase” model was originally proposed by Doufas *et al.*, 1999, 2000 and followed by Zheng and Kennedy 2004). The flow-induced stresses are relatively small, but they contribute to orientation which influences the thermal and mechanical properties, and hence the shrinkage and warpage behavior of the molded parts. The second source of the residual stresses is the thermally and pressure-induced stresses, which arise during the packing and cooling stages, and make the main contribution to the total residual stresses. Details of the thermally and pressure-induced stress equations and numerical solution schemes for their calculation have been described by Zheng *et al.* (1999). However, one also needs to incorporate the predicted processing-induced morphology and crystallinity into the calculation to achieve anisotropic thermal and mechanical properties. To do this, we use the Mori-Tanaka model and treat the spherulites and shish-kebabs as inclusions embedded in an amorphous matrix. For a review of several micromechanical models, the reader is referred to Tucker and Liang (1999).

3. Material and Experiments

3.1. Material selection

A primary aspect of this work is focused on modeling the influence of colorants on the crystallization kinetics and anisotropic shrinkage of the injection-molded parts. We have chosen to use an iPP (grade HD601CF, supplied by Borealis) as the virgin material and two different types of blue colorants as additives. The virgin material is transparent and its properties are given in Table 1.

The two types of blue colorants are Sodium Alumino Sulpho Silicate (commercial name: Ultramarine Blue) and Cu-Phthalocyanine (commercial name: PV Fast Blue), both supplied by Clariant Australia. We denote them as UB colorant and CuPc colorant, respectively. The UB colorant is inorganic, having a light blue color and a spherical surface full of holes of a uniform size, while the CuPc-colorant is organic, having a dark blue color and a flat surface full of narrow cracks of nonuniform sizes. Each colorant was pre-mixed with the base material in a blender at room temperature and then in a twin screw extruder at 220°C, with a concentration of 0.8% by weight. The extruded strands were immediately quenched into water and then cut into pellets. The samples were labelled as PP, PP+08U, and PP+08P, where PP stands for the virgin material, “08” stands for the concentration of

Table 1. Material properties of Borealis HD601CF IPP

Parameter	Symbol	Value
Molecular weight (weight average)	M_w	367 kg/mol
Molecular weight distribution	M_w/M_n	4.96
Melt Flow Rate (230°C, 2.16 kg)	MFR	8 g/10 min
Glass transition temperature	T_g	264 K

Table 2. Equilibrium melting temperatures T_m^0 for three samples.

PP	PP+08U	PP+08P
206°C	189°C	177°C

0.8% , and "U" and "P" stand for the UB colorant and the CuPc colorant, respectively.

3.2. Quiescent crystallization parameters

3.2.1. Equilibrium melting temperature

Differential scanning calorimetry (DSC) was used to determine the equilibrium melting temperature, T_m^0, by the Hoffman-Weeks extrapolation method (Hoffman and Weeks 1962). The value of T_m^0 corresponds to the intersection of the experimental $T_m = f(T_c)$ line and the first diagonal $T_m = T_c$, where T_m is the melt point obtained by heating the sample at a rate of 10°C/min, after the sample was isothermally crystallized at a constant temperature T_c. As an example, Fig. 1 shows the determination of the equilibrium melting temperature for the virgin iPP. Melting point data (T_m) were obtained on the samples isothermally crystallized at temperatures ranging from 120.4°C to 153.4°C. Despite the fact that one might regard the equilibrium melting temperature as an intrinsic parameter of the polymer crystal, our experimental measurements (Table 2) show some variation with additives.

In an independent experiment for the same materials, Zhu et. al. (2009) obtained $T_m^0 = 205°\text{C}$ for both PP and PP+08U, and $T_m^0 = 179°\text{C}$ for PP+08P. Considering that the two independent experiments were done by different experimenters with different DSC apparatuses, the discrepancies between the two sets of experimental results are not very large.

3.2.2. Half crystallization time

For measuring the quiescent half crystallization time ($t_{1/2}$), again the DSC was used. The sample was melted and maintained at 210°C for 5 minutes to remove crystallization and pre-processing history, then was cooled at a rate of 30°C/min to a desired crystallization temperature, T_c. At this temperature, the sample was held until sufficiently crystallized. The time-dependent relative crystallinity was calculated by integrating the area inside the DSC crystallization curve. Then the half crystallization time corresponding to temperature T_c was obtained for a relative crystallinity $\alpha = 0.5$. Fig. 2 shows an example for sample PP for T_c = 128, 132, 136, and 140°C.

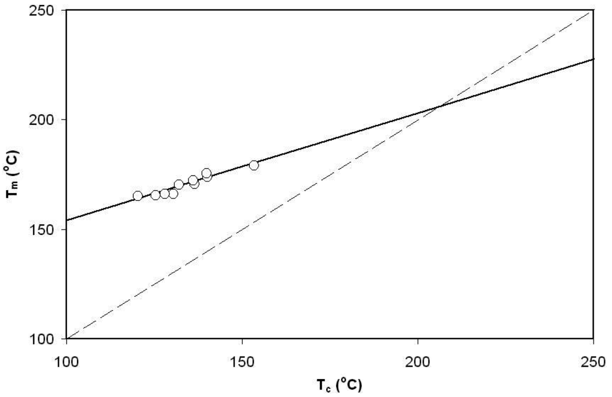

Fig. 1. Determination of equilibrium melting temperature for sample PP by the Hoffman-Weeks extrapolation method.

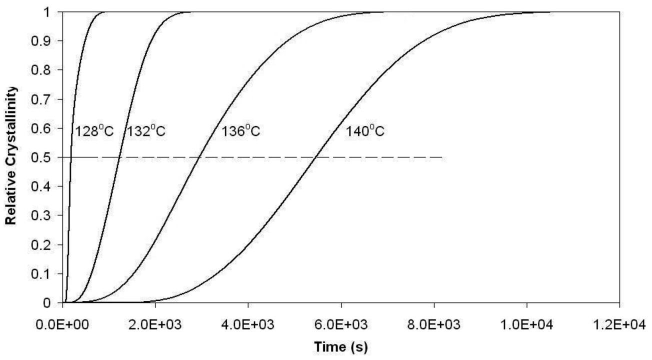

Fig. 2. Determination of the half crystallization time at different temperatures for the virgin iPP.

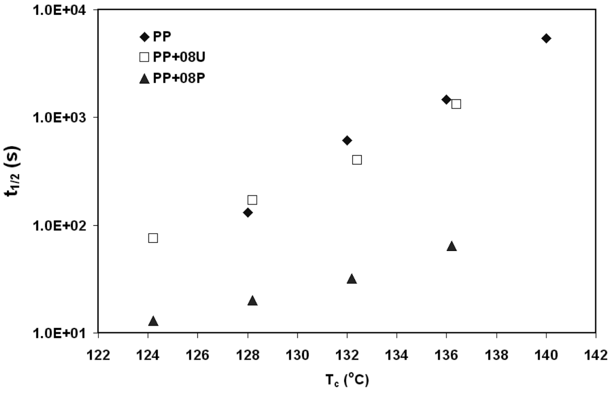

Fig. 3. Half crystallization time vs. crystallization temperature for three samples.

Experimental results for the three samples are plotted in

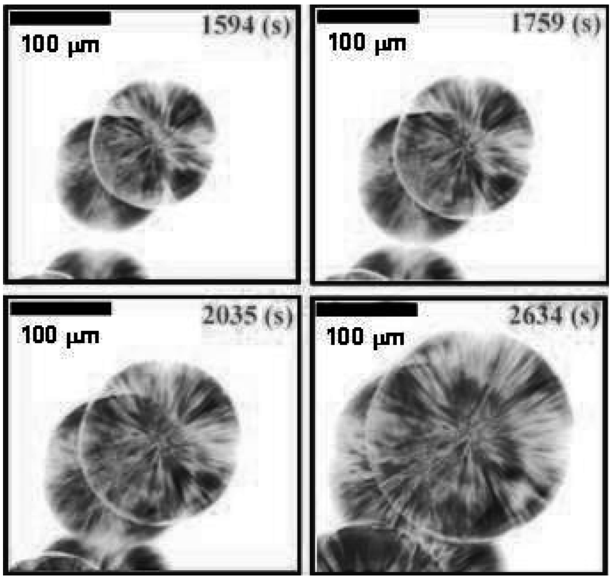

Fig. 4. Growth of spherulites observed under microscopy for the virgin iPP sample at 135°C.

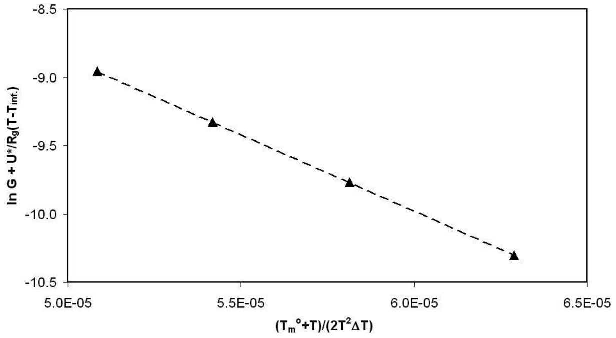

Fig. 5. Determination of constants G_0 and K_g for sample PP+08P.

Fig. 3. The results show that the crystallization speed is slightly influenced by the UB colorant but dramatically enhanced by the CuPc-colorant. The half crystallization times of the CuPc-colored material are smaller by one order of magnitude than the corresponding half crystallization times of both the virgin iPP and the UB-colored material.

3.2.3. G(T) and N_0(T)

Fig. 4 shows optical microscopy images of the crystallizing PP sample at temperature 135°C, at different times. Such images were used to measure the average spherulite radius versus time at different temperatures. The time interval for the photos can be 30 s, 60 s, or 300 s depending on the speed of crystallization. The linear fit of the radius vs. time gives the spherulite grow rate $G(t)$. The constants G_0 and K_g in the Hoffman-Lauritzen equation (Eq. 4) were determined by plotting $\ln G+(U^*/R_g)(T-T_\infty)$ against $(T+T_m^0)/2T^2\Delta T$, given U^*=6270 J/mol and T_g = 264 K for all the 3 samples. Fig. 5 shows an example of determining G_0 and K_g for sample PP+08P where $G_0 = 3.82\times10^{-2} m/s$ and $K_g = 1.12\times10^5 K^2$ were obtained. The constant K_g is known to be associated with the energy barrier for the formation of a critical nucleus. We obtained $K_g = 7.15\times10^5 K^2$ for the virgin iPP, and $K_g = 3.76\times10^5 K^2$ for the UB-colored iPP.

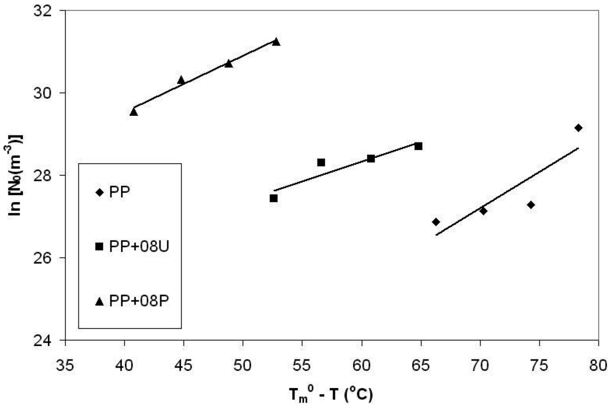

Fig. 6. Quiescent nuclei number densities of the virgin iPP and the colored iPPs with UB colorant and CuPc colorant.

Table 3. Parameters a_N and b_N

	PP	PP+08U	PP+08P
a_N	0.176	0.095	0.137
b_N	14.86	22.60	24.05

Although the microscopic images could also be used to count the nuclei number per unit volume, $N_0(T)$, the nucleation of the PP+08P sample occurs too fast and the resolution of the microscopic images is too poor to provide an accurate value for $N_0(T)$. We hence calculate the $N_0(T)$.from the known G(T) and $t_{1/2}(T)$ using the following equation:

$$N_0 = \frac{3\ln 2}{4\pi G^3 t_{1/2}^3} \tag{24}$$

which is derived from the Avrami equation (Eq. 6). Having obtained $N_0(T)$, the parameters a_N and b_N in Eq. (7) can be determined by linear regression. Nucleation curves under atmospheric pressure for the 3 samples are given in Fig. 6. The values of a_N and b_N are summarized in Table 3.

3.2.4. Specific heat capacity

The specific heat capacity at constant pressure, c_p, is measured by performing cooling scans with a DSC for the three samples, from 240°C to 30°C with a cooling rate of 20°C/min. The heat capacity curves are shown in Fig. 7. Both UB and CuPc colorants increase the magnitude of the peak in the c_p curves. Further more, the figure shows that the positions of the peaks of the virgin iPP and the UB-col-

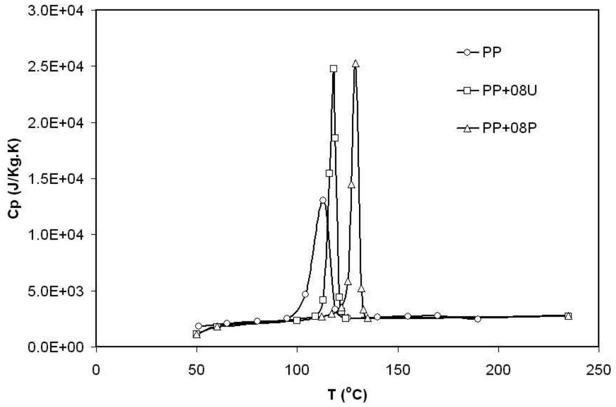

Fig. 7. Specific heat capacity of three samples.

Table 4. Latent heat of crystallization for three samples.

	PP	PP+08U	PP+08P
ΔH_c (J/kg)	95000	99295	103925

ored iPP vary by 5°C. However the CuPc colored sample has a peak 16°C above that of the uncolored iPP and so significantly reduces the degree of supercooling.

The crystallization latent heat can be estimated from the area under the peak; the values are listed in Table 4.

3.2.5. Ultimate absolute crystallinity

The Ultimate absolute crystallinity (χ_∞) estimated from WAXS results are 0.53, 0.58 and 0.66 for PP, PP+08U and PP+08P, respectively. We take an approximate value of $\chi_\infty = 0.6$ for all the three samples in the numerical simulations.

3.3. Flow-induced crystallization parameters

A Linkam shearing hot stage combined with microscope and light intensity reader was used to determine the half crystallization time after shear. The experimental procedure can be summarized as follows:

1. The sample is put into the Linkam Cell, melted, and pressed to a thickness of 0.1 mm.
2. The sample is annealed at 210°C for 5 minutes.
3. The sample is cooled to the desired crystallization temperature with a cooling rate of 30°C/min.
4. As soon as the temperature is reached, a step shear is applied for a short period, denoted by t_s, and at different shear rates ranging from $0 \sim 100\ \mathrm{s}^{-1}$.
5. The change in polarized light intensity with time is recorded, and the experiment is finished when the intensity reaches a stable value, indicating that crystallization is completed. From the change in intensity, the half crystallization time as a function of shear rate can be determined.

It is thus possible to use the experimental data to determine the parameters associated with the flow-induced crystallization model.

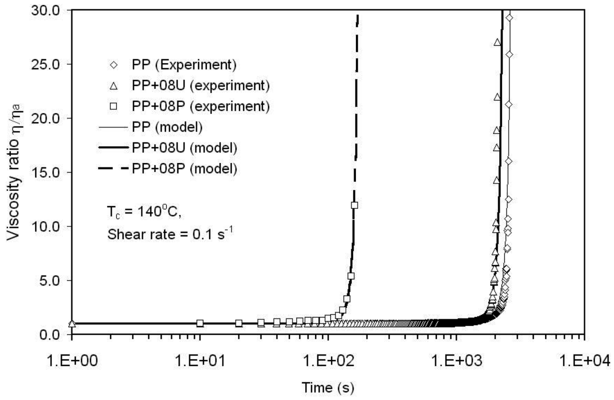

Fig. 8. Experimental and modeled viscosity ratios for three samples in steady shear at T_c=140°C and $\dot{\gamma}$= 0.1 s^{-1}.

Table 5. Parameters β and β_1 in Eq. (15) ($A = 0.44$)

	PP	PP+08U	PP+08P
b	3.7	3.7	12
β_1	1	1	1

We have noted that a careful choice of the experimental crystallization temperature is essential. If the temperature is too high, the crystallization process will be too slow and make the experiment impractical. On the other hand, if the chosen crystallization temperature is too low, then the crystallization induction time will be too short and make the measurement of the intensity of the transmitted light difficult or inaccurate, We chose two crystallization temperatures, $T_c = 132$°C and 136°C in the experiments for the virgin and the UB-colored iPP. This range of crystallization temperatures allowed convenient experimental times for the two samples. However we had to choose higher temperatures for the CuPc-colored iPP, because it crystallized too fast at low temperatures. The temperatures chosen for the CuPc-colored sample were $T_c = 144$°C and 148°C. Experimental results will be reported later together with modeling results.

3.4. Viscosity

Steady shear experiments with a parallel plate rheometer were performed to monitor the effect of crystallization kinetics on viscosity. More details on the experiments were reported elsewhere by Lee Wo and Tanner (2010). In this study we fit Eq. (15) to the experimental data to determine the model parameters β and β_1 for using in simulations. Fig. 8 shows an example of the model fitting. The model parameters obtained are given in Table 5.

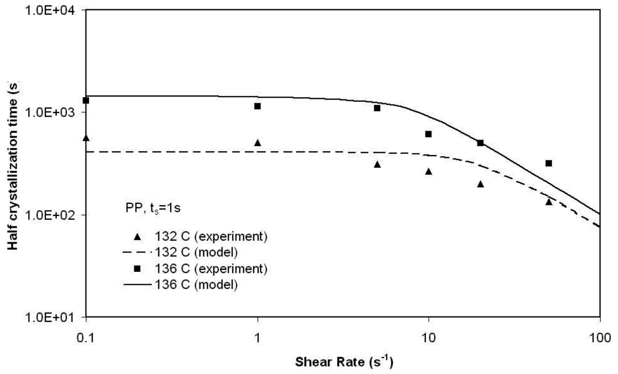

Fig. 9. Experimental and simulated half crystallization time versus short-term shear rate for the virgin iPP at two crystallization temperatures and a fixed shearing time of 1 sec.

There was a difficulty in the experiments when the sample solidified. In this case the sample tends to shrink and may detach from the wall of the plates of the rheometer, indicated by a sudden drop or an oscillation in the viscosity-time curve. This usually occurs when $\eta/\eta_a > 10$ (the upturn in viscosity has already taken place) and hence has little influence on the determination of β and β_1.

3.5. Shrinkage measurement

Experimental shrinkage data are required for investigating effects of the colorants on the properties of the final products, and also for experimental validation of numerical simulations. The injection-molded samples are fan-gated rectangular plates, 200 mm long and 40 mm wide. The thickness of the samples are 1.7 mm, 2 mm, 3 mm and 5 mm. We applied a set of 28 processing conditions to mold each sample. The set of processing conditions include different combinations of sample thickness, melt temperature, mold temperature, flow rate, holding pressure, holding time and cooling time, These were described by Kennedy and Zheng (2006) in more detail. The molded plates were stored for 10 days at room temperature to reach their final level of crystallinity and stable geometry of the moldings. In-plane shrinkages of the parts were then measured in two directions, one along the direction parallel to flow, and the other perpendicular to the flow direction.

4. Results and Discussions

4.1. Enhancement of crystallization speed

Figs. 9, 10 and 11 show the experimental and simulated half crystallization times after shear as a function of the shear rate at different temperatures for PP, PP+08U and PP+08P, respectively. The figures demonstrate the ability of the FIC model to describe correct trends for both the influences of shear rate and temperature, and for materials with and without colorants.

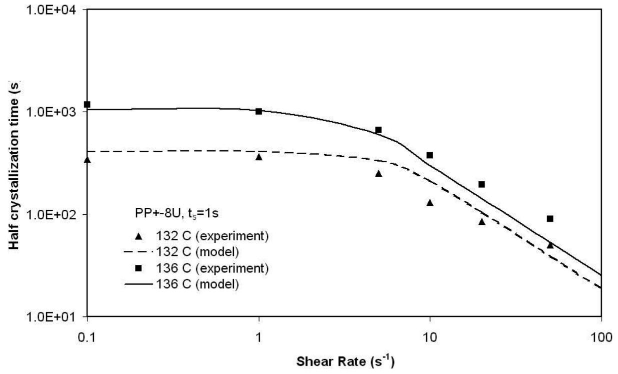

Fig. 10. Experimental and simulated half crystallization time versus short-term shear rate for the UB-colored iPP at two crystallization temperatures and a fixed shearing time of 1 sec.

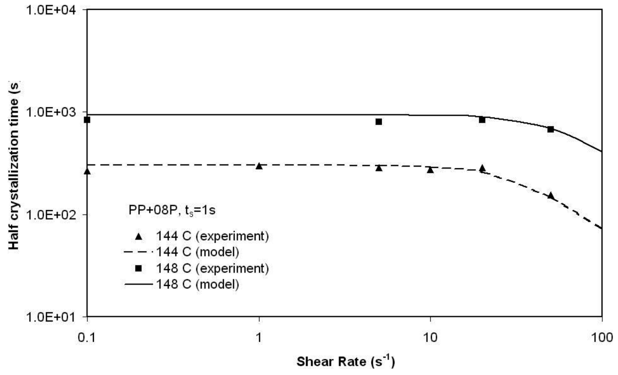

Fig. 11. Experimental and simulated half crystallization time versus short-term shear rate for the CuPc-colored iPP at two crystallization temperatures and a fixed shearing time of 1 sec.

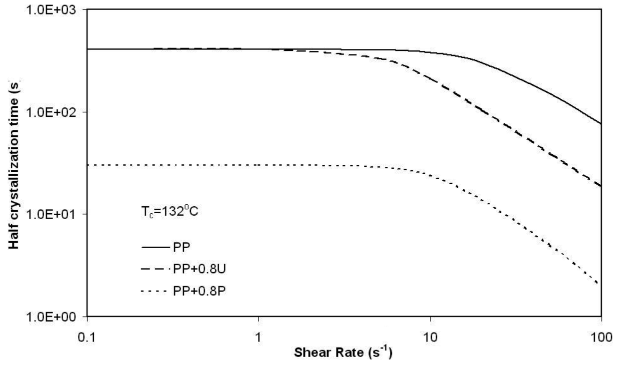

Fig. 12. A comparison of simulated half crystallization times versus short-term shear rate for the three samples at $T_c = 132^{\circ}\mathrm{C}$ and $t_s < 1\mathrm{s}$.

As mentioned in the previous section, in the Linkam shearing experiment, we had to test the sample PP+08P in the higher temperatures compared to those used for PP and PP+08U. This raises a difficulty for comparison. However, the FIC kinetic model can be used to predict $t_{1/2}$ at the same

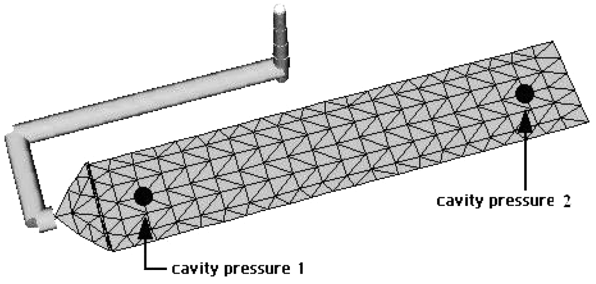

Fig. 13. Finite element mesh of the fan-gated rectangular part and the pressure measurement points.

temperature for all three samples. Fig. 12 shows the predicted results for all samples at $T_c = 132^\circ\mathrm{C}$. One can see that the nucleating effect of the UB colorant is negligible for quiescent and low shear-rate ($\dot{\gamma}<1s^{-1}$) crystallization, but becomes significant for flow-induced crystallization at higher shear rates. Thus, the UB colorant tends to increase the sensitivity of crystallization to shear. Compared to the UB colorant, the CuPc colorant is highly effective as a nucleating agent even in the quiescent state.

As the UB colorant has negligible influence on the quiescent crystallinity of the iPP, its influence on the flow-induced crystallization was somewhat unexpected. This phenomenon may be attributed to the local shear rate concentration. Although the virgin iPP and the UB-colored iPP have similar level of half crystallization times in quiescent conditions, we did observe from the microscopy that the two samples have quite different morphology, especially in the nuclei distribution and the nuclei number density (see Lee Wo and Tanner 2010). Therefore, when the samples are sheared, the local effective shear rates in the two samples will be different for the same applied shear rate.

4.2. Cavity pressure in injection molding

In this study, cavity pressure evolution is measured for the previously mentioned fan-gated rectangular parts for the experimental validation of numerical predictions. Pressure profiles were measured at two points as shown in Fig. 13. As an example, we show here the part with 2 mm thickness. For all three materials, the melt was injected with a constant flow rate of $3.7\times10^{-5}\,m^3/s$ at 202°C, and the mold temperature was set to 41°C. The packing pressure at the nozzle was maintained at 30.5 MPa for a holding time of 20 s before it dropped to zero, then followed by a cooling time of 10 s.

A finite element method was employed to solve a two-dimensional pressure equation using a mid-plane mesh, while a finite difference scheme was used to solve the three-dimensional temperature field. This method, often referred to as 2.5D analysis, was documented in detail by Kennedy (1995).

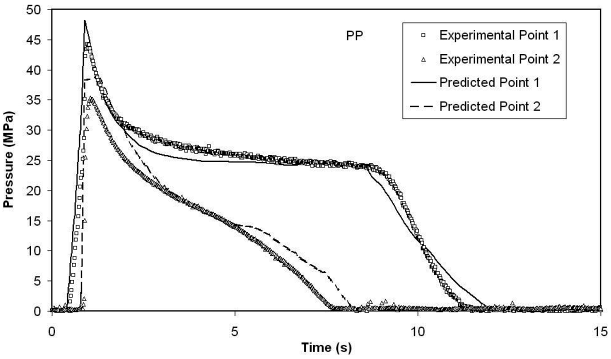

Fig. 14. Measured and predicted pressure profiles for the virgin iPP.

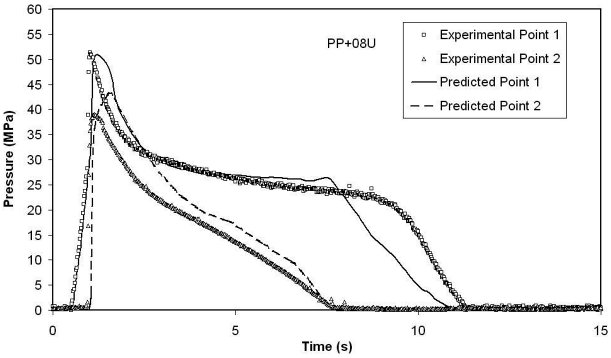

Fig. 15. Measured and predicted pressure profiles for PP+08U.

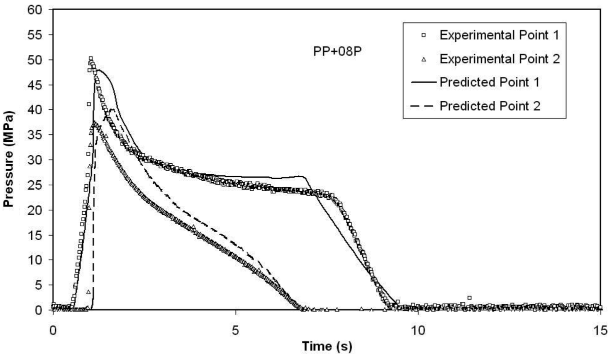

Fig. 16. Measured and predicted pressure profiles for PP+08P.

Experimental and predicted pressure profiles are shown in Figs.14, 15, and 16 for the PP, PP+08U and PP+08P samples, respectively. The pressure measured just downstream from the gate (Point 1) can give an indication about the solidification evolution at the gate. The beginning of the pressure decay is due to the gate freezing and is an indicator of effective temperature and viscosity modeling. From the figures, we found that the CuPc colorant causes the pressure to decay earlier; this phenomenon is consistent with its effect on speeding up crystallization.

The cavity pressure prediction is sensitive to variations

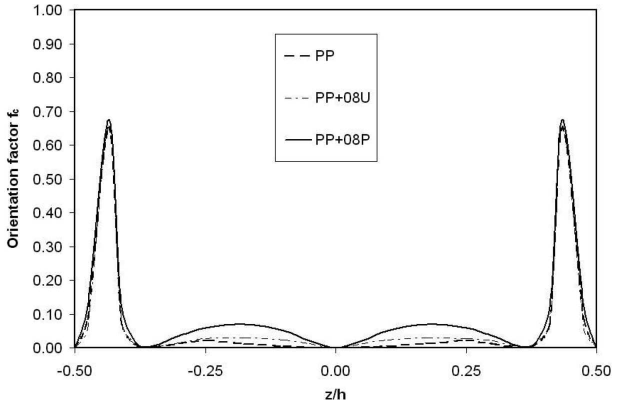

Fig. 17. Gap-wise Orientation factor profiles for PP, PP+08U and PP+08P.

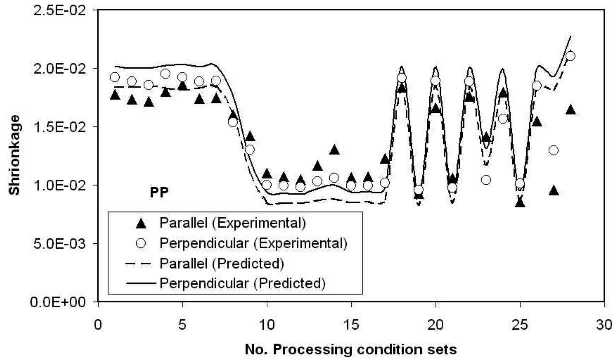

Fig. 18. Experimental and predicted parallel and perpendicular shrinkage for the virgin iPP.

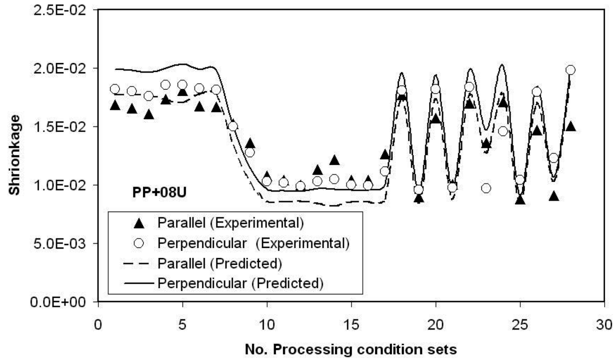

Fig. 19. Experimental and predicted parallel and perpendicular shrinkage for the iPP colored by UB colorant.

of thermal diffusivity $k/\rho c_p$, which is a function of crystallinity. Higher values of diffusivity will speed up the pressure decay. Viscosity upturn due to crystallization also greatly changes the pressure transmission and evolution. Flow-induced crystalline orientation has little effect on the pressure profile but significantly affects shrinkage results. In addition, it is also known that the mold deformation and the heat transfer coefficient at the polymer/mold interface also influence the agreement of the predictions with measurements.

4.3. Orientation factor

The Herman's orientation factor f_c is often used as a quantitative measure of uniaxial orientation. The value of f_c can be calculated in injection molding simulation and it gives us information about the distribution of microstructure, either oriented or isotropic. In particular, $f_c = 0$ corresponds to a random orientation and an isotropic microstructure, $f_c = 1$ indicates a highly oriented structure which is perfectly aligned in the flow direction, and $f_c = -0.5$ signifies an orientation perpendicular to the flow direction.

Fig. 17 shows the predicted gap-wise profiles of the orientation factor f_c for the 2 mm-thick plates as used above for the pressure calculations. The molding conditions were also the same as described above. Results for the three materials were all taken from the element located at the center of the plate. A typical layered structure is observed. The first layer is at the polymer/metal interface, where a nearly zero f_c is predicted. Moving inward from the surface, there is a highly oriented layer, where the material experienced high shear-rate flow action and then froze due to rapid crystallization that preserved the orientation in the flow direction. When the cavity is full, the flow rate generated by packing is much lower than in the filling stage, and the shear stresses in the molten polymer layer decay quickly. Therefore, further inward from the high shear region, there is a minimum in the crystalline orientation function, which is followed by a second hump. The second hump was developed during the post-filling stage. As the solid/melt interface moves inward, a small flow rate in a narrower channel may still result in a considerable deformation. Moreover, due to the decreasing temperature with time (which leads to higher viscosity and relaxation time), even small shear rates may still introduce high stresses and lead to oriented structures. Finally, around the symmetry plane, where the shear rate is approximately zero, the orientation factor drops to zero as expected, implying isotropic spherulitical structures in the core region of the part. Such kinds of five-layered structure have been observed in experiments by Mendoza *et al.* (2003).

4.4. Shrinkage

Measured and predicted shrinkages (parallel and perpendicular to flow direction) are shown in Figs. 18 to 20, respectively, for the three samples. The undulation of the data reflects the influence of the processing conditions on the shrinkage of the moldings. For a few processing conditions, the agreement between the experimental data and numerical prediction is not entirely satisfactory in magnitude, but nevertheless the predicted results match the experimental trends and in most cases the magnitudes.

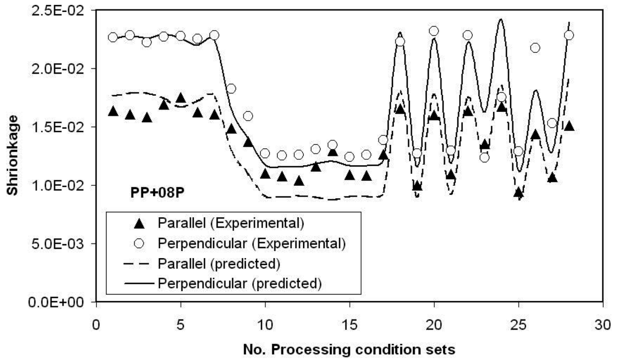

Fig. 20. Experimental and predicted parallel and perpendicular shrinkage for PP colored by CuPc colorant.

Comparing the three figures, of particular note is the higher degree of anisotropy exhibited by the CuPc-colored iPP, which was correctly predicted by the present model.

5. Conclusions

In this study, we perform experiments and numerical simulations to investigate the effects of two colorants on flow-induced crystallization and anisotropic properties of injection molded parts. The two colorants have different particle geometries and surface patterns. The CuPc colorant with flat surfaces has shown to be a very effective nucleating agent in both quiescent and flow conditions. Moreover, it results in a higher degree of anisotropy in shrinkage. The UB colorant with spherical surface is not effective in the quiescent conditions but increases the sensitivity to pre-shear effects. It does not lead to anisotropic shrinkage. A basic FIC model with the parameters determined separately for different samples gave a good prediction of the colorant effects observed in experiments.

Acknowledgements

We acknowledge gratefully the (Australian) Polymer Cooperative Research Centre for the financial support, Borealis GmbH, Linz, Austria for the supply of material, Moldflow Plastics Laboratory of Autodesk Pty. Ltd., Melbourne for providing experimental apparatus and material characterization.

References

Avrami, M., 1939, Kinetics of phase change, I. General theory, *J. Chem. Phys.* **7**, 1103-1112.

Dai, S.C., F. Qi. and R.I. Tanner, 2006, Strain and Strain-Rate Formulation for Flow-Induced Crystallization, *Polym. Eng. Sci.* **46**, 659-669.

Dai, S.C. and R.I. Tanner, 2006, Anisotropic thermal conductvity in sheared polypropylene, *Rheol. Acta*, **45**, 228-238.

Doi, M. and S.F. Edwards, 1986, The Theory of Polymer Dynamics. Clarendon Press, Oxford.

Doufas, A.K., I. S. Dairanieh and A. J. McHugh, 1999, A continuum model for flow-induced crystallization of polymer melts, *J. Rheol.* **43**, 85-109.

Doufas, A.K., A. J. McHugh and C. Miller, 2000, Simulation of melt spinning including flow-induced crystallization, Part I. Model development and predictions, *J. Non-Newtonian Fluid Mech.* **92**, 27-66.

Eder, G. and H. Janeschitz-Kriegl., 1997, Crystallization, in *Materials Science and Technology,* Vol. 18, Processing of Polymers (H. E. H. Meijer, ed.), Wiley-VCH, New York.

Fan X-J., 1985, Viscosity, first normal-stress coefficient and molecular stretching in dilute polymer solutions, *J. Non-Newtonian Fluid Mech.* **17**, 125-144..

Fulchiron, R., E. Koscher, G. Poutot, D. Delaunay and G. Regnier, 2001, Analysis of the Pressure Effect on the Crystallization Kinetics, Dilatometric Measurements and Thermal Gradient Modelling. *J. Macromolecular Science – Physics* **40**, 297-314.

Hadinata, C., R. Zheng, P.K. Kennedy, P. Zhu, G. Edward, D. Lee Wo and R. I. Tanner, 2008, The effects of additives on material properties and shrinkage characteristics, *Proc. PPS-24* Salerno.

Hoffman, J. D. and J. J. Weeks, 1962, Melting process and the equilibrium melting temperature of polychlorotrifluoroethylene, *J. Res. Natl. Bur. Stand* **66A**, 13-28.

Housmans, J.W., M. Gahleitner, G.W.M. Peters and H.E.H. Meijer, 2009, Structure-property relations in molded, nucleated isotactic polypropylene, *Polymer* **50**, 2304-2319.

Huilgol, R.R., N. Phan-Thien and R. Zheng, 1992, A theoretical and numerical study of non-Fourier effects in viscometric and extensional flows of incompressible simple fluid, *J. Non-Newt. Fluid Mech.* **43**, 83-102.

Kennedy, P.K., Flow Analysis of Injection Molds, Hanser, Munich, (1995).

Kennedy, P.K. and R. Zheng, 2006, Shrinkage of injection molded material, in *Precision Injection Molding: Process, Materials, and Applications,* edited by Jehuda Greener and Reinhold Wimberger-Friedl, Hanser, 105-135.

Kolmogoroff, A. N., 1937, On a statistical theory of crystallization of melts, *Bull, Akad. Sci. USSR, Class Sci., Math. Nat.* **1**, 355-359.

Koscher, E. and R. Fulchiron., 2002, Influence of shear on polypropylene crystallization: morphology development and kinetics, *Polymer* **43**, 6931-6942.

Lauritzen, S.I. and J. D. Hoffman, 1960, Theory of formation of polymer crystals with folded chains in dilute solution, *J. Res. Natl. Bur. Stand.* **64A**, 73-102.

Lee Wo, D. and R.I. Tanner, 2010, The impact of blue organic and inorganic pigments on the crystallization and rheological properties of isotactic polypropylene, *Rheol. Acta* **49**, 75-88.

Mendoza, R., G. Régnier, W. Seiler and J.L. Lebrun., 2003, Spatial distribution of molecular orientation in injection molded iPP: influence of processing conditions, *Polymer* **44**, 3363-3373.

Mykhaylyk, O.O., P. Chambon, R.S. Graham, J. Patrick, A. Fairclough, P.D. Olmsted and A. J. Ryan, 2008, The Specific Work of Flow as a Criterion for Orientation in Polymer Crystallization, *Macromolecules* **41**, 1901-1904.

Pantani, R., I. Coccorullo, V. Speranza and G. Titomanlio, 2005. Modeling of morphology evolution in the injection molding process of thermoplastic polymers, *Prog. Polym. Sci.* **30**, 1185-1122.

Silberman, A., E. Raninson, I. Dolgopolsky and S. Kenig, 1995, The effect of pigments on the crystallization and properties of polypropylene, *Polymers for Advanced Technologies* **6**, 643-652.

Tanner, R. I., 2003, On the flow of crystallizing polymers, I. Linear regime, *J. Non-Newtonian Fluid Mech.* **112**, 251-268.

Tanner, R.I. and F. Qi, 2005, A comparison of some models for describing polymer crystallization at low deformation rates. *J Non-Newton Fluid Mech.* **127**, 131-141.

Tucker, III C.L. and E. Liang, 1999, Stiffness predictions for unidirectional short-fiber composites: Review and evaluation. *Comp Sci Technol.* **59**, 655-671.

Vanden Brule, B.H.A.A., 1989, A network theory for the thermal conductivity of an amorphous polymeric material, *Rheol. Acta*, **28**, 257-266.

Van Meerveld, J. 2004, A method to extract the monomer friction coefficient from the linear viscoelastic behavior of linear, entangled polymer melts, *Rheol. Acta* **43**, 615-623.

Van Meerveld, J., G., W. M. Peters and M. Hütter, 2004, Towards a rheological classification of flow induced crystallization experiments of polymer melts, *Rheol. Acta* **44**, 119-134.

Zheng, R. C. Hadinata and P. Kennedy, 2008, Numerical study on the impact of additives on shrinkage of injection molded polypropylene, *The XV International Congress on Rheology, Monterey, AIP Conf. Proc.* **1027**, 45-47.

Zheng, R. and P. K. Kennedy, 2004, A model for post-flow induced crystallization: general equation and predictions,” *J. Rheol*. **48**, 823-842.

Zheng, R. and P.K. Kennedy, 2006, Anisotropic thermal conduction in injection molding, *Proc. 22nd Annual Conference of the Polymer Processing Society*, Yamagata, Japan.

Zheng, R., P.K. Kennedy, N. Phan-Thien and X.J. Fan, 1999, Thermoviscoelastic simulation of thermally and pressure induced stresses in injection molding for the prediction of shrinkage and warpage for fibre-reinforced thermoplastics, *J. Non-Newtonian Fluid Mech.* **84**, 159-190.

Zhu, P., A. Phillips and G. Edward, 2009, Experimental observation of effects of seeds on polymer crystallization, *Physical Review E.* **80**, 051801.

Zuidema, H., G.W.M. Peters and H.E.H. Meijer, 2001, Development and validation of a recoverable strain based model for flow-induced crystallization of polymers, *Macromol. Theory Simul.* **10**, 447-460.